Eur. Phys. J. B **7**, 585–597 (1999)

THE EUROPEAN PHYSICAL JOURNAL B

EDP Sciences

Edge of disorder

Analysis of disordered polymers: polyaniline

M. Laridjani[1,a] and A.J. Epstein[2]

[1] Laboratoire de Physique des Solides[b], Université de Paris-Sud, 91405 Orsay Cedex, France
[2] Department of Physics and of Chemistry, The Ohio State University, Columbus, OH 43210-1106, USA

Received: 7 May 1997 / Revised: 2 July 1998 / Accepted: 25 September 1998

Abstract. Polyanilines belong to a family of electronic polymers. Due to a wide range of variable parameters in the synthesis of polyanalines, a variety of samples with different physical properties can be achieved. Different investigators have identified the degree of crystallinity for different varieties of polyanilines. They have classified them into two classes of emeraldine forms. In these structural investigations, the traditional "concept of the two phase system" was used for differentiating the crystalline phase. Recently, it has been shown that washing the emeraldine base (EB) by NMP or THF will establish two different X-ray patterns. The X-ray pattern of the sample washed with THF shows a limited number of Bragg lines superimposed on the broad diffuse halos. Other patterns only indicated broad diffuse halos. These experimental facts do not advocate the "two phase system model", especially with scarce Bragg reflections. We have set-up an elegant prototype for X-ray diffractometry which allows us to obtain a high resolution X-ray pattern from polymers with coherent intrinsic backgrounds. Formally, this *coherent* background was excluded for polymer structural identification. Nevertheless, we have introduced a new method of separating the reflected lines from a *coherent* background. The interference functions $F(K)$ of the coherent background were obtained applying this novel technique. The advantage of our method of separation is verified by comparing the background of $F(K)$ with the $F(K)$ of the sample washed with NMP. Fourier inversion is used to identify the short range order of the atoms responsible for the diffuse scattering. This result enabled us to choose a standard state of disorder in polymers. This standard state of randomness can be considered as the *edge of disorder*. By defining this reference state of randomness, it can be seen that the atomic arrangements of long and fast changing structural chains correspond best to the random array model rather than the two phase system model. The novel experiment and analysis technique presented here offer a possibility of application of structural studies to many common polymers, all of which have the characteristic of the diffuse halo underlying the diffraction lines.

PACS. 61.43.Dq Amorphous semiconductors, metals, and alloys – 61.43.Er Other amorphous solids – 61.41.+e Polymers, elastomers, and plastics

1 Introduction – chemical evolution of polyaniline

The study of the polyaniline family of electronic polymers began nearly a century ago. This study has been intensified for the past decade [1]. Schema 1 shows the general composition of the base form of polyaniline where its average oxidation state is given by the parameter, $(1-y)$. When $y \sim 0.5$ the material is called an emeraldine base (EB). The electrically conducting emeraldine salt is obtained by protonic acid doping of the emeraldine base [2].

The interpretation of the relationship of the physical phenomena associated with each sample relative to its preparative conditions is a very difficult task due to the wide variety of parameters in the synthesis and processing routes when different types of emeraldine are prepared [2, 3]. The degree of polymerisation and the *self-organisation* of the resulting polymer chains as they come out of solution are sensitive functions of the polymerization conditions. In addition, protonation procedures using a variety of protonated acids can be used to change the emeraldine oxidation state of the polymer from an insulating

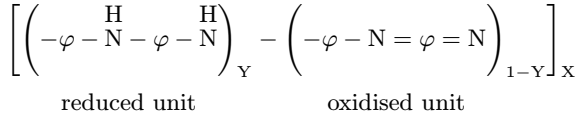

Schema 1. An illustration of the reduced and oxidized repeat units of polyaniline.

[a] Corresponding author (Fax: 331 69 15 60 86).
[b] URA 02 – CNRS

emeraldine base (EB) ($\sigma \cong 10^{-10}$ Ω^{-1}/cm) [4] to a conducting metallic emeraldine (ES) ($\sigma \cong 10^{+2}$ Ω^{-1}/cm [5, 6]) through protonation with a wide variety of protonated acids. Finally, the sample can be in the form of a powder or a film. Structural studies provide a means of establishing the local order which has resulted from different types of chemical reactions.

Recently structural studies by classical X-ray diffraction have been performed on the polyanilines. As a result two classes of emeraldine have been reported [7,8].

Usually, class I is obtained from an acid solution of the doped emeraldine salt (ES) form. Dedoping ES-I leads to an amorphous insulating emeraldine base (EB-I). The X-ray pattern of EB-I consists of overlapping broad diffuse halos. The EB-I powder may be transformed to EB-II powder by *washing* with tetrahydofuran (THF) or N-methylpyrolidinone (NMP) solution and subsequently drying under vacuum. X-ray diffraction patterns of EB-II show sharp lines superimposed over diffuse halos. These lines have been indexed as an ordered system [7,8]. For EB-II (as well as doped ES-II) the estimated relative intensity of the sharp lines for unstretched EB-II and ES-II varies with each sample preparation.

In our initial studies of polyaniline, the traditional concept of artificially separating the crystalline and the amorphous state was used to differentiate the crystalline state from the amorphous state.

Emeraldines have been obtained in a wide variety of degrees of order. Even for "amorphous" emeraldines the presence of diffuse halos show that a short range order exists. Hence the use of two discrete "phases" in the structural analysis is questioned [9,10].

The structural analysis of diffraction data for polymers presents the following problems:

(a) The variation of the intrachain configuration for one end of a polymer chain to the other end. This variation can lead to a *"continuous transition"* from a well ordered portion to a strongly disordered portion of a chain. This leads to broadened diffraction lines (halo).
(b) Polymers that consist of light elements, principally C, N, and H. This leads to relatively enhanced incoherent X-ray scattering (Compton radiation) which will obscure coherent scattering.
(c) The diffraction line profile varies by increasing 2θ.
(d) The three effects above (a–c) cause the intrinsic diffraction pattern from the polymer samples to appear relatively *featureless*. It follows that contributions made by incoherent scatterings from other sources (such as air, sample holders, *etc.*) can cause significant effects.

2 Experimental technique

A diffractometer has been designed to adapt to the parallel beam of a high intensity source (rotation-target diffraction tube or synchrotron radiation). This diffractometer consists of three main parts: a goniometer, an energy calibration, and data acquisition with Processing Software. In transmission and reflection geometry, the goniometer can be used for θ-2θ scanning with a resolution $\theta = 0.001°$. The parallel beam is obtained by a slit system proposed by Guinier *et al.* [12] for the small angle scattering technique. Hence, the scattered radiation for a very small Bragg angle, θ, is not overshadowed by the direct beam. Depending on the information required from the samples, the geometrical condition and optical arrangements of the diffractometer can be optimised. In this special set-up, the goniometer can be used in dispersive and non-dispersive modes. In the dispersive mode, a polychromatic component of X-ray radiation is used, θ and 2θ are fixed. In the non-dispersive mode, the monochromatic component of X-ray radiation is used in order to obtain X-ray diagrams with different wavelengths, in the same experiment. For the separation of the fluorescence and the incoherent radiation from a coherent component, the scattered beam is recorded by a new prototype energy dispersive detector which is connected to a Preamplifier and a Plus Processor. The energy selection can be performed by two different procedures. The first procedure is to use a flat monochromator (Si, Ge, C, LiF) providing rapid tunability over a white spectrum. The energy calibration is achieved by step scanning across the absorption edge of the element in the specimen. The second procedure is performed by a scattered beam from a substance that can be selected by a programmed multichannel software as an energy window.

We have used a non-energy dispersive technique with high intensity, different wavelengths, and a parallel beam to obtain the X-ray patterns of the different polyanilines. This technique facilitates the important background and Compton scattering corrections for obtaining high quality X-ray diffraction patterns with very high resolution. The parallelism of incident X-ray beams and the geometry of the diffractometer help to eliminate several corrections such as the effect of sample size or the effect of sample shape. This ease of wavelength selection allows us to acquire the patterns with a chosen wavelength near or far from the atomic absorption edges, consequently allowing an easy absorption correction for reflection or transmission geometries and a direct use of high (hkl) reflection to determine lattice parameters for perfectly ordered systems.

The ease of wavelength selection also allows to obtain high quality interference functions ($J(K)$) for systems with a low degree of order, including polymers. This high quality interference function deviates from the coherent intensity, ($I_C(K)$), that would be generated by all the atoms of polymers scattering independently of one another (see Eq. (1)). The high quality interference functions and the ease of wavelength selection yield structural information about the environment of each component within the substance. This technique is based on an anomalous dispersion effect and permits us to obtain partial interference functions, using the rapid change of the atomic scattering factor (f) of one atomic species. The atomic scattering can be written as:

$$f(K,E) = f_0(K) + f'(K,E) + if''(K,E).$$

Here f_0 is the atomic scattering factor for radiation with a frequency (ω) higher than the (ω) of the absorption edge.

The other two terms of anomalous dispersion depend on $E = \hbar\omega$. The techniques of this method are described in references [31,32].

A reasonable interference intensity can be registered from the correlation of the first and second atomic shells especially in disordered materials, with light atoms, such as polyaniline. But the intensity of interference beyond the second shell is not very high and any aberration can be a cause of error. This is a reason for caution in X-ray pattern analysis. The advantage of the use of the interference function is to be able to arrive at an integrated model instead of the two phase system models of crystal and amorphous structure.

Non-energy dispersive diffractometry with a parallel beam

In this technique a diffractometer has been adapted for use with a parallel X-ray beam. In order to separate fluorescent and incoherent radiation from the coherent component, $I_C(K)$, the scattered beam is recorded by a novel energy dispersive detector which is connected to a preamplifier and a pulse processor. The pulse processor is a sophisticated signal processing unit which provides linear amplification, noise filtering, pulse pile-up rejection and life-time correction. The combination of these functions is an essential prerequisite for achieving accurate X-ray analysis. The pulses are accumulated in a multichannel analyser interfaced to a computer. The solid state detector has an energy resolution of 150 eV at 8 keV and 230 eV at 20 keV. Its high resolution in energy not only permits the elimination of fluorescent radiation from the sample but also partially removes the incoherent Compton scattering.

The novel diffractometer is mounted on a rotating Rigaku target of an Ag X-ray source. The sample was scanned from $2\theta = 1°$ to $90°$ (*i.e.* from $K = 0.4$ Å^{-1} to 15 Å^{-1}) in transmission geometry and reflection geometry ($2\theta = 1°$ to $125°$) (*i.e.* from $K = 0.4$ Å^{-1} to 20 Å^{-1}). In the present study only the $\lambda_{K\alpha} = 0.560\,9$ Å wavelength was analysed.

Hence, the part of the diagram ($2\theta < 60°$) that was acquired by transmission and the other part of the diagram ($2\theta > 60°$) that was obtained by reflection geometry were used to obtain a more precise $I_C(K)$.

The effective elimination of the Compton scattering is better achieved by selecting the half-profile of the higher energy of the $\mathrm{Ag}_{K\alpha}$ characteristic spectrum. As the value of K increases there is less and less overlap between the coherent and Compton profiles. For large K values (above 7 Å^{-1} in our case) the Compton peak can be totally separated. The upper half profile of K_α almost completely consists of the coherent component. Figure 1 shows the two $I_C(2\theta)$'s of the EB-II form of polyaniline with and without Compton scattering. In this respect the energy analysis method has been taken the place of an ideal monochromator in the diffracted beam. For smaller K values this technique leads only to a partial removal of the Compton

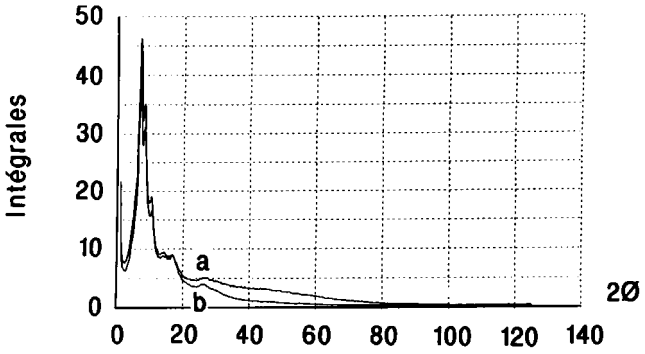

Fig. 1. The X-ray diagrams of polyaniline, (a) X-ray pattern $I_C(2\theta)$ of the EB-II with compton radiation (incoherent radiation) and (b) the X-ray pattern of EB-II without compton radiation (see text).

scattering. At low K values (below 5 Å^{-1} in our case) the Compton contribution to the K_α profile is negligibly small compared to the strong coherent intensity scattered by the polymer. Thus there is a small range of K values where the experimental data must be corrected in order to eliminate completely the Compton scattering. This has been done by a classical procedure of normalisation.

Only the coherent part of the diffracted intensity $I_C(K)$ is used in the analysis of the atomic arrangement in amorphous structures. The interference function $J(K)$ is defined by:

$$J(K) = \frac{I_C(K)}{Nf^2(K)}\cdot \tag{1}$$

Here, $K = 4\pi \sin\theta/\lambda$ is the scattering vector, N is the number of all identical atoms that scatter independently; except for fluctuations of $(P(x) - 1)$.

$P(x) = \rho(r)/\rho_0(r)$ is defined as an atomic distribution where $\rho(r)$ is the atomic density and $\rho_0(r)^{-1} = v$, the mean atomic volume. $J(K)$ can be expressed in the Debye approximations in the following form:

$$J(K) = 1 + \int_0^\infty 4\pi r^2 \left[\rho(r) - \rho_0\right] \frac{\sin Kr}{Kr}\, dr\cdot \tag{2}$$

By defining the reduced radial distribution function it is easy to show:

$$W(r) = r[P(r) - 1]. \tag{3}$$

Then, (2) can be written as:

$$F(K) = K\left[J(K) - 1\right] = 4\pi\rho_0 \int_0^\infty W(r)\sin Kr\, dr. \tag{4}$$

Equation (5) defines the reduced interference function $F(K)$ as related to $W(r)$ by Fourier Transformation:

$$W(r) = (2\pi^2\rho_0) - 1 \int_0^\infty F(K)\sin Kr\, dr. \tag{5}$$

The function $W(r)$ was deduced from the data correction and the analytical normalisation of $F(K)$ using the Kaplow correction procedure. We took into consideration that there are no inter atomic distances smaller than the nearest neighbouring distances. Therefore indicating that the curve below the first peak of $W(r)$ has a slope of "-1". We have succeeded in obtaining such a slope by changing the correction parameters. For further detail ([9,13,31]) should be referred to.

Expressions (1–5) apply to a monoatomic *isotropic* amorphous material. This is nearly the case of the polyaniline emeraldine base form of the polyaniline (Schema 1 above, with $y = 0.5$) because the carbon and nitrogen atoms have similar "form factors" and the X-ray scattering by the hydrogen atoms is negligible.

Sections 1 and 2 describe the basic principles of data collection conditions used for our amorphography experiments. These conditions have also been reported in our previous publications.

3 Results

In order to increase the reliability a repeated number of scans, typically 15, were taken for each sample, to minimise any small variations in the X-ray patterns. The X-ray patterns ($I_C(2\theta)$) of different emeraldine base samples (EB) can be classified into two types:

(a) the first type only contains a few broad diffuse halos without any detailed structure. Some of these patterns show the presence of a very small peak before the first diffuse halo, termed here the "pre-peak". There is a similarity between the diffuse X-ray patterns of this type (a). The following features occur frequently in type (a) samples:
   (i) a characteristic width of the principle halo at the half-maximum intensity;
   (ii) the first halo position and its shape can serve as a first test for finding the degree of disorder in polyaniline;
   (iii) a pre-peak exists in some samples;

(b) the second type (b) of X-ray patterns consists of sharp lines superimposed on the diffuse halos.

This classification is relevant to the polyaniline in both the *powder and the film form*.

The degree of disorder of various samples can be determined by comparing the details of the diffraction profile of the first halo of each sample of type (a). For instance, the existence of the pre-peak is a valid signature for the evolution of disorder. For X-ray patterns of type (b), with halo and sharp lines, it would be convenient to separate the sharp lines from the halo (background). Due to the law of conservation of intensity, *i.e.* the amount of intensity scattered by the sample can be determined by integration of volume over the square of electron density, $\rho^2(r)$, independent of how the atoms are distributed in space.

4 The separation procedure of the sharp lines from the broad halos

A crucial step for the structural study of polymers is the separation of the sharp lines from the background of the X-ray patterns. Usually, Ruland's [14,15] method is recommended for the separation of the crystalline phase from the amorphous phase in various polymers (the two phase system concept). This method requires the knowledge of the *diffraction curve shape of the amorphous phase* [16,17]. Where possible the intensity scattered by the strongly disordered (amorphous) polymer should be measured precisely.

For ideal powder diffractometry, with random orientation of the crystallites in the polymer, a strict monochromatic beam and ideal X-ray optics are recommended. However, such performance in classical X-ray diffractometry would be a difficult task. Here, a new procedure is proposed [18] in which the diffraction pattern has been numerically resolved into halos and sharp lines by a computer program utilising the following three hypotheses.

(a) The law of conservation of coherent intensity applies for X-rays scattered by polymers. This means that the intensity (I) of each point in the X-ray diagram is the sum of the intensity scattered by the crystal part (I_C) and the amorphous part (I_A) in the polymer. Then:

$$I_{Total} = I_C + I_A. \tag{6}$$

(b) The intensity of each point of the amorphous diffraction curve should be:

$$I_A \leq I_{Total}. \tag{7}$$

(c) The intensity of any point of the X-ray pattern where there is no line should be:

$$I_C = 0 \quad \text{and} \quad I_A = I_{Total}. \tag{8}$$

By using these hypotheses the sections of the diffraction curve without sharp lines will be incorporated as a part of the amorphous curve and the portion obscured by the sharp lines will be extrapolated by interpolation. If the two phase concept is utilised, the sharp lines are considered representative of the crystalline X-ray diagram.

The MATLAB (toolbox of 3860) program [19] has been expanded for these computational operations and linear interpolations. Briefly, these operations consist of selecting a real point of amorphous diffraction intensity, on the $I_C(2\theta)$ curve and comparing its magnitude with the mean I of the previous point. The missing part of amorphous X-ray diagram is constructed point by point and this procedure is shown in Figure 2. The resolution and profile of an amorphous diagram obtained by this program is linked to the number of times the operation is run and the resolution of the steps for computational averaging. With this method of separation two sets of spectra are obtained. One is a line spectrum and the other a halo spectrum.

As a result the spectrum of lines can be compared by measuring the relative intensity, the maximum position

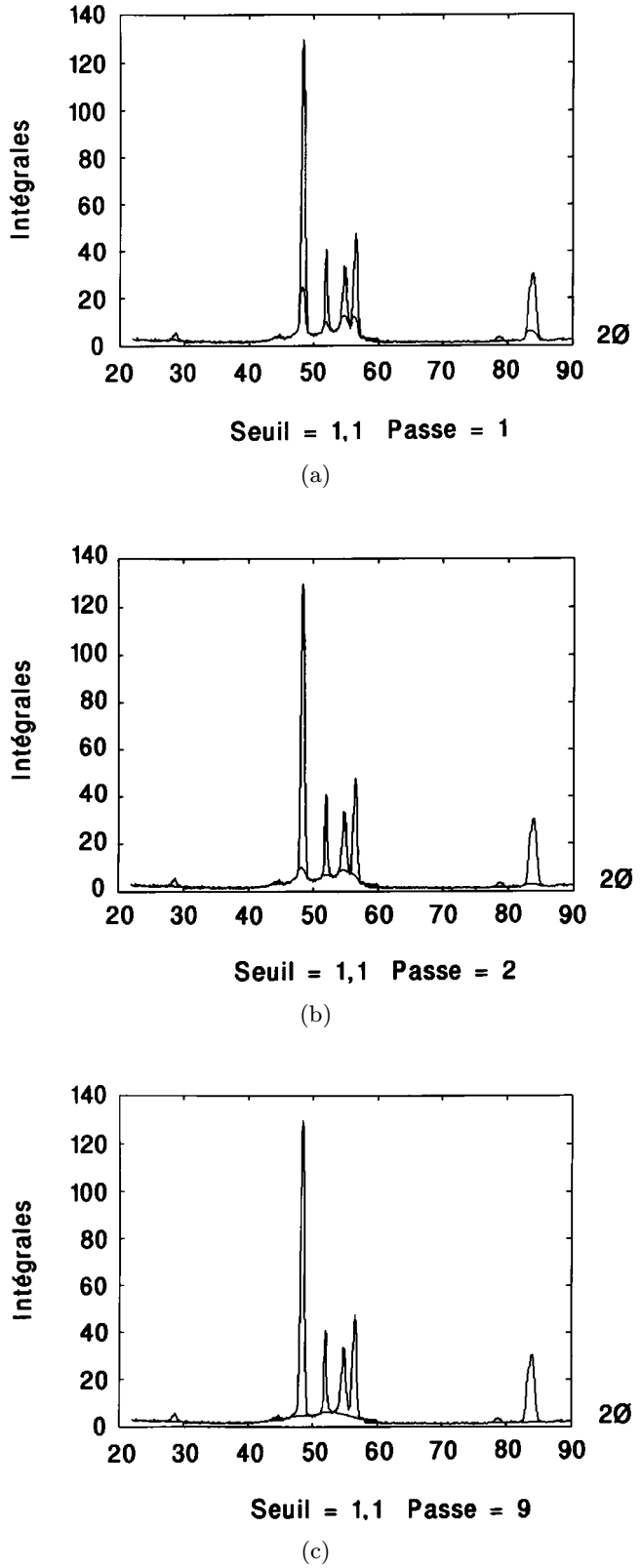

Fig. 2. This figure indicates the separation procedure to obtain line spectra and diffuse halos (*cf.* [18]); (a) the initial state of separation; (b) intermediate state of separation; (c) the final state of separation of lines from the broad halos (coherent background).

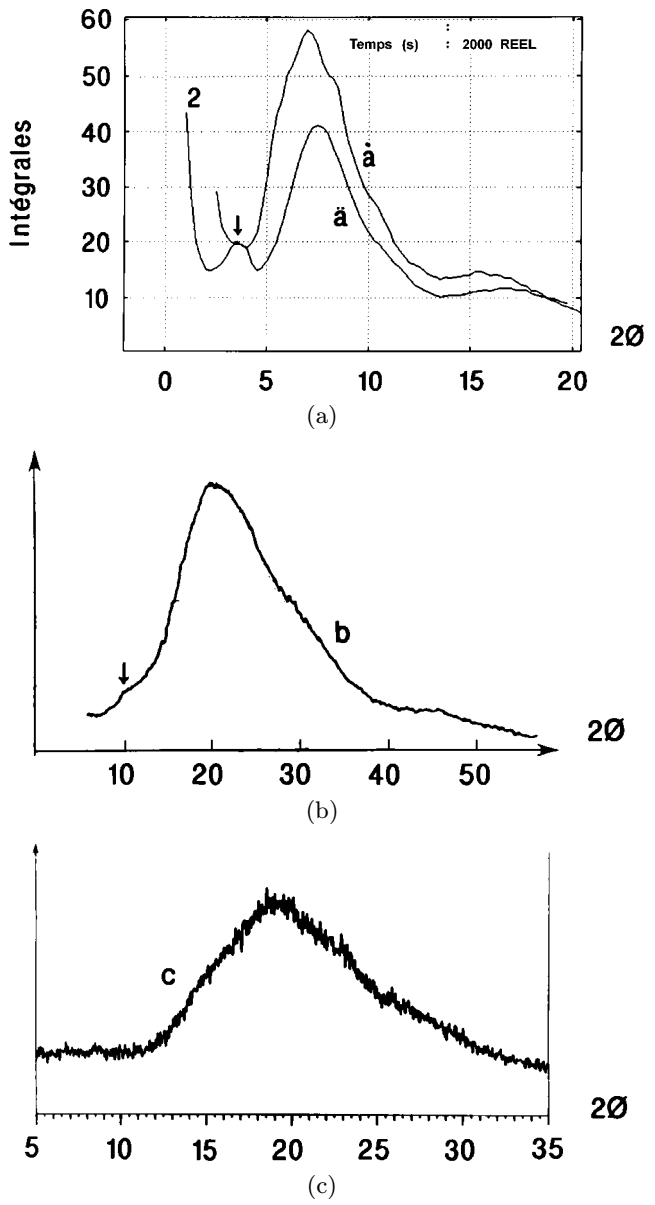

Fig. 3. The diffracted intensity, $I_C(2\theta)$, scattered by various emeraldine bases; obtained by different X-ray technique: (a) achieved by anomalous diffractometry using parallel beams with $\lambda = 0.506\,9$ Å (à–sample *without* pre-peak (EB-I), ä–sample *with* pre-peak (EB-I)); (b) an X-ray pattern of EB-I, obtained by a Debye Scherrer camera using synchrotron radiation $\lambda = 1.596$ Å [8]; (c) an X-ray pattern of the same sample of (ä) obtained by conventional diffractometry with $\lambda = 1.54$ Å; however, here there is no evidence of the pre-peak (see text).

and the profile of each line. Here the relative intensity can be defined as the ratio of the integrated intensity of each line to the integrated intensity of the strongest line. Hence, a related structure factor $F(hkl)$ of each line can be obtained accurately in contrast to that obtained before the separation procedure.

Figure 3 indicates a series of X-ray diffraction patterns of various polyanilines obtained by different

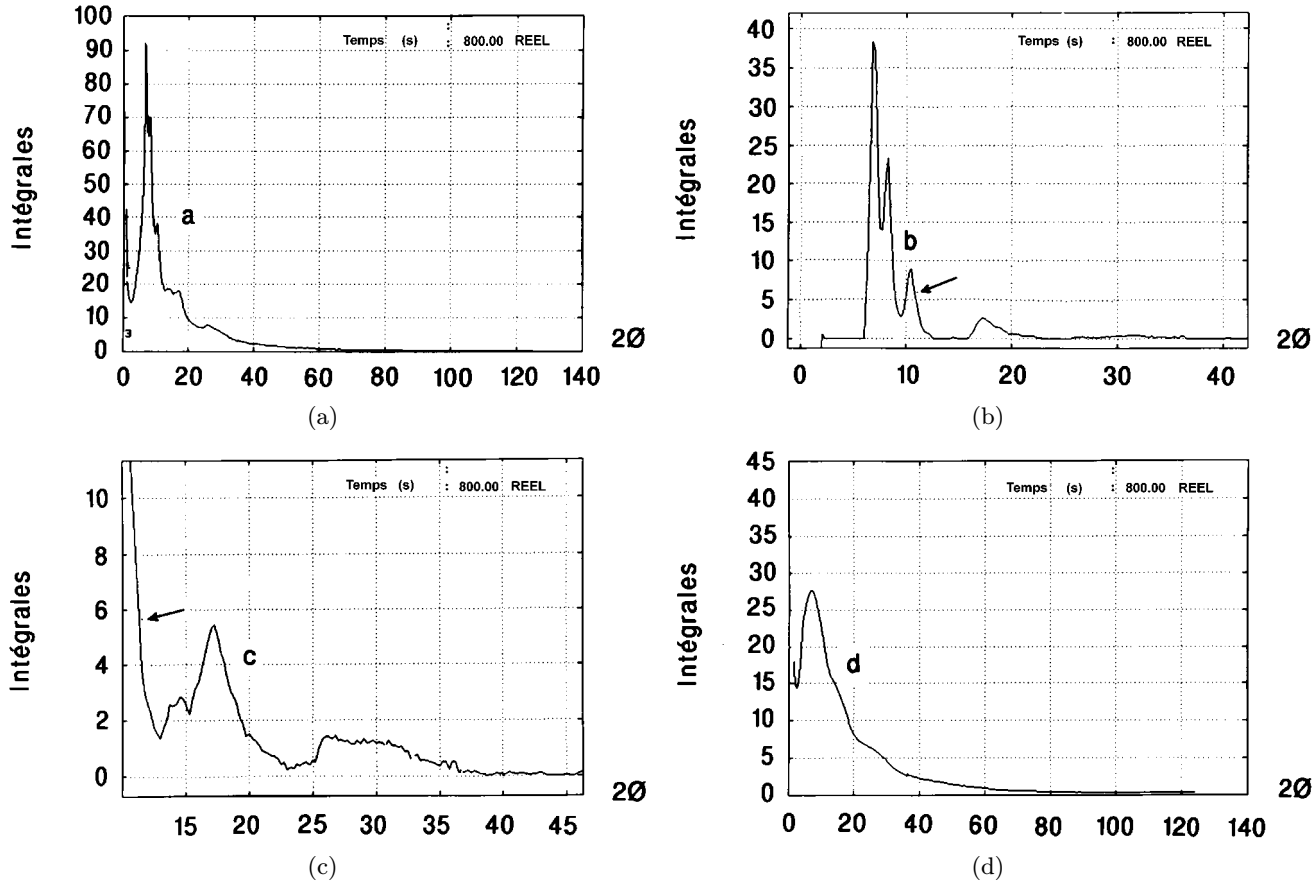

Fig. 4. The X-ray pattern of the emeraldine base, washed in THF solution. (a) This figure shows no evidence of the pre-peak but there are sharplines superimposed on the broad diffuse halos (mixed pattern); this X-ray diagram has been classified as a (type b). (b) X-ray diagram of line spectra after separation from the broad halos. (c) is (b) zoomed from $2\theta = 10°$. For verification of each line profile. There is a drastic change, of profile with no similarity to Bragg line profiles. This profile change is in the form of diffraction bands (see text). (d) The spectrum of broad halos after separation from lines; *i.e.* the coherent background of X-ray pattern of EB-II (Fig 4a).

techniques. Figure 3a shows the X-ray pattern of two insulating polyaniline (EB) samples that were obtained by dedoping [3,7,9] emeraldine hydrochloride (ES-I) salt powder, by *washing* with 0.1 M NH_4OH solution. It can be seen that the features of the $I_C(2\theta)$ curve are the same except for the presence of a very small peak prior to the first principal halo at $2\theta = 3°$ for $\lambda = 0.560\,9$ Å (Fig. 3a (ä)). Due to the parallel incident beam the pre-peak can be easily observed here. In this method scattered radiation, for very small Bragg angles (θ) from the sample, is not overshadowed by a direct beam. This peak can also be observed in Figure 3b as reported earlier by Pouget *et al.* [8]. That diffraction pattern, Figure 3b, was obtained by a Debye-Scherrer camera using synchrotron radiation where the beam is also a parallel beam. In this Debye-Scherrer pattern the method of sample preparation was not the same and the half-maximum peak breadth was different to the one obtained in the present work.

When an EB-I powder is *washed* by THF, the pre-peak disappears and sharp lines superimposed on the broad halos appear (see Fig. 4a). This diffraction pattern supports that the sharp lines are intrinsic to the samples washed by

Fig. 5. The Guinier pattern of two EB-I samples. The beams are monochromatic (CuK_α): (a) X-ray pattern of the same sample as ȧ; (b) X-ray pattern of the same sample as ä; this figure shows clearly small angle scattering with pre-peak.

THF and do not result from specimen preparation in the sample holder of the diffractometer. By using the Guinier technique, the existence of the pre-peak is also checked for EB-I in its powder form. In the Guinier camera the powder form is not mechanically stressed. The powder samples have an effective thickness of $1/\rho\mu_0$ where ρ is the density and μ_0 is the X-ray linear absorption coefficient [13]. With such a technique a powder specimen with strictly

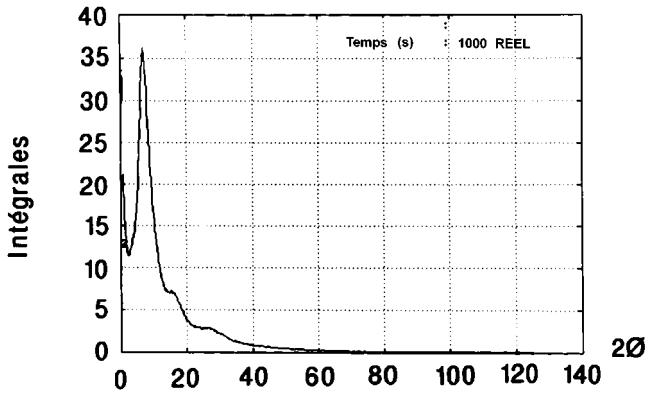

Fig. 6. The X-ray pattern of an emeraldine base, washed with NMP solution. This X-ray diagram is typical of spectra of *pure amorphous* polyaniline (type a) (see text). The resemblance of this diagram to Figure 4d (coherent background) confirms the validity of this separation procedure.

random orientations can be obtained. Figure 5 shows a Guinier pattern for two powder samples of EB-I obtained by washing ES-I. The pre-peak can be observed in Figure 5a.

Figures 3a and 3c compare two X-ray patterns of the *same sample*. One sample is with the pre-peak and the other without. The pattern of 3a is recorded by a conventional diffractometer (Bragg-Brentano) with $\lambda = 1.54$ Å. A conventional diffractometer does not allow the pre-peak to be observed because the pre-peak would be overshadowed by a direct beam.

The sample may also be in the form of a film. The film form can be obtained by dissolving the emeraldine base in NMP and then casting it on a glass substrate. The X-ray pattern of the film and powder forms are illustrated respectively in Figures 6 and 4a. No evidence of a pre-peak or sharp lines is seen in Figure 6. These patterns indicate that the structure of this polymer can be changed by just *washing* the powder with solvents such as THF and NMP.

Figure 4b shows the line spectra obtained by the separation method which give a set of line reflections. Up to $2\theta = 25°$ for $\lambda = 0.560\,9$ Å the lines are symmetrical and beyond this value they become very large and asymmetrical (see Fig. 4c).

The "*d*" spacings and the relative intensity of each line from this set is compared to the "*d*" spacing and the *estimated intensity* reported by Pouget *et al.* [8]. This comparison indicates the same result for the calculated value of "*d*". For this list of "*d*" spacings an orthorhombic unit cell has been proposed (*cf.* Tab. 1).

Figure 4d shows a "spectrum of broad" halos (*coherent background*) after separating the sharp lines from the mixed pattern (see Fig. 4a). The behaviour of the X-ray pattern obtained from the sample, in film form, prepared by dissolving the insulating EB-I powder with NMP can be compared to the coherent background spectrum. The broad halo pattern scattered by disordered atoms can be considered as the X-ray diffraction pattern of *pure amorphous* polyaniline (Fig. 6).

Table 1. The position of reflected lines in the washed EB-I powder spectrum. The first three columns are results from this paper (Fig. 4b). The last three columns are from Pouget *et al.* [8].

2θ	Photon number (I)	d (Å)	Pouget *et al.* [8] d (Å)	Pouget *et al.* [8] I	hkl
6.25°	42 357	4.75	4.56	*vs*	(110)
8.5°	20 353	3.78	3.83	*s*	(200)
			3.41	*vw*	(112)
10.5°	11 140	3.06	3.02	*m*	(211)
			2.82	*w*	(020)
13.75°	2 052	2.34	2.33	*w*	
14.5°	2 265	2.22	2.19	*w*	(114) (221)
17.25°	4 363	1.87	1.84	*w*	(321) (115)
					(130)
20°	1 207	1.6			
22.75°	337	1.36			
23.75°	300	1.406			
26.5°	1 041	1.223			
30.25°	942*	1.074			
31°	?*				
33.25°	588*				
36.25°	384*				
37.25°	137*				
40.25°	132*				
46.5°	137*				

d (Å) has been obtained by $2d \sin\theta = \lambda$, with $\lambda = 0.560\,9$ Å. The profile of the lines beyond $2\theta = 25°$ for AgK_α are not similar to Bragg reflections *i.e.* asymmetrical profile or band form profile.

* Because of the shape of the lines a significant measurement could not be performed.

By comparing these two patterns of the coherent background for the EB-I powder (Fig. 4d), and the EB-I film sample, (Fig. 6), it can be concluded that the coherent diffracted intensity is from the disordered part of the polyaniline. This broad diffraction pattern of coherent background indicates the same state of randomness as the pure amorphous phase and can be considered as the isotropic state of bulk polyaniline which is strongly disordered.

This new technique of X-ray diffractometry proves that the primary effect of preparative conditions appears with long range (profile of the first peak) and medium range correlations (existence of the pre-peak). This technique is very convenient for characterising polymers by comparing their $I_C(2\theta)$ and taking into consideration the coherent background.

The various $I_C(2\theta)$'s are used to classify the X-ray patterns of polyanilines. This classification varies from the large halo pattern to the mixed type (sharp lines with halos). Each diagram can be considered as a "*fingerprint*" of each sample. Therefore the study of the physical properties of polymers for their eventual applications can be carried out more easily. The separation procedure precisely

classifies the line spectrum for each sample and this may help to achieve a classification scheme for the polymers.

5 The reduced interference function F(K)

Here we address the relationship between the origins of the sharp lines and the broad halos. We have utilised amorphography techniques which require high quality interference functions [9,10].

Figure 7 displays the reduced interference function, $F(K)$, of different samples of emeraldine base derived from diffracted intensities $I_C(2\theta)$. Although these figures qualitatively look alike, there are distinct quantitative differences on the interference function of EB-I (Fig. 7). Before the first principal diffuse peak (halo) at $K = 0.5$ Å^{-1} a pre-peak can be observed on the interference function of EB-I (Fig. 7a). This principal peak of $F(K)$ is usually associated with the far atomic correlation shell and it shows the presence of structural regularity in the long range correlation. The half-maximum breadth of this diffuse peak at $K \sim 1.5$ Å^{-1} indicates the degree of atomic disorder of the far shell. In all interference functions of emeraldine an asymmetrical profile of this peak is the main characteristic. This asymmetrical shape occurs because of the presence of a small shoulder on the high K side which is not very well resolved from the principal peak of $F(K)$.

In the proposed model for liquid benzene the same appearance has been observed in the reduced interference function, $F(K)$. This phenomenon has also been observed experimentally. Narten has reported [20] that the theoretical interference function can be calculated by assuming the same local order in liquids as in crystalline solids [21]. Figure 8 shows how well, in the reciprocal space, the theoretical $F(K)$ of liquid benzene, for a very large domain of K ($K = 10$ Å^{-1}), fits with EB-II's (in film form (Fig. 7d)) reduced interference function.

The difference in the case of benzene is that the shoulder is well resolved both in the experimental procedures and the theoretical models. The comparison of the interference function of the EB-II emeraldine base (Fig. 7d) with the calculated $F(K)$ of benzene indicates an essential agreement in behaviour despite the differences in the profile and the peak heights. However, the profile of the principal peak informs us, in general, about the similarity of order in the long range correlation of liquid benzene and pure amorphous emeraldine base. This essential agreement in the behaviour of liquid and EB-II's $F(K)$ reminds us of Bernal's approach to the structure of liquids. He considers that a liquid is a loosened solid with a different "*fundamental irregularity*" and reports that their structural irregularity is responsible for the liquids' properties shown by the X-ray diffraction pattern evolution [22].

A more difficult problem is the analysis of the medium range correlation. It is worthwhile comparing the second and the third peak of different functions. These peaks can be related to the medium range order (MRO). In all interference functions of different emeraldines the maximum position of the second peak before and after being *washed*,

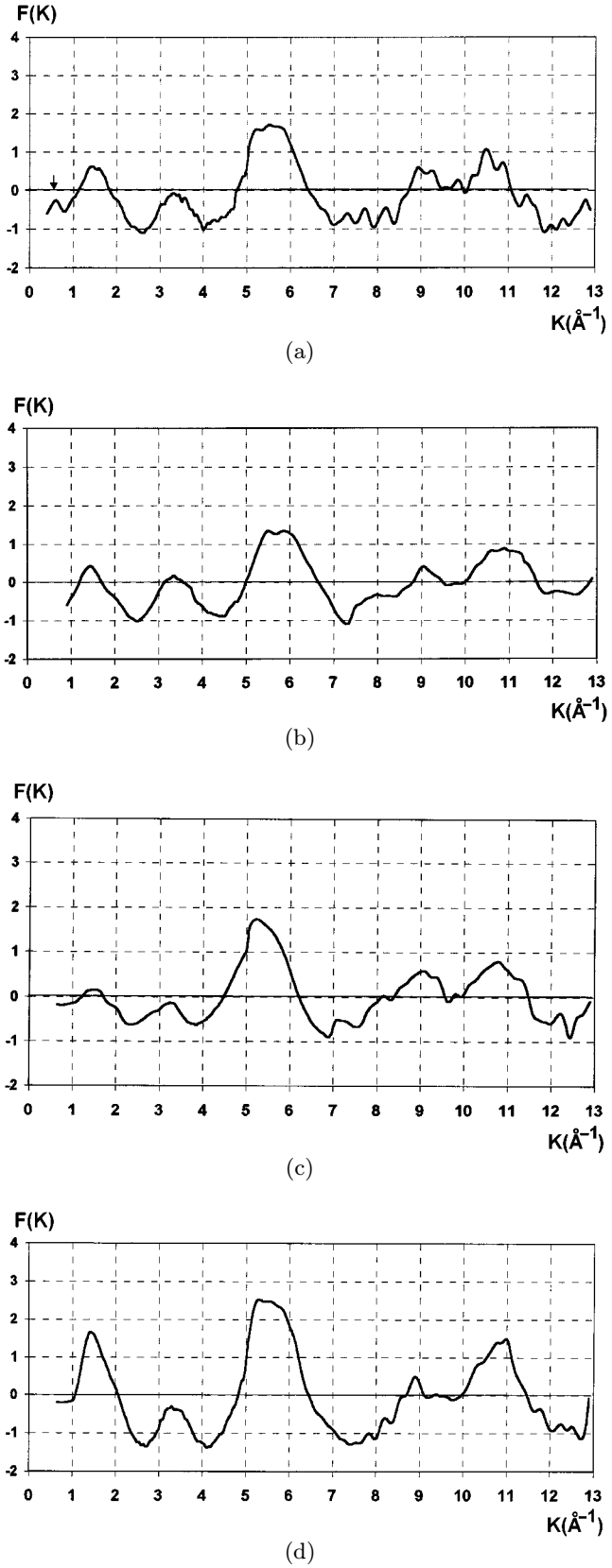

Fig. 7. The reduced interference function derived from diffracted intensities ($I_C(2\theta)$): (a) $F(K)$ of EB-I with pre-peak derived from ($I_C(2\theta)$) of Figure 4a (ä); (b) $F(K)$ of EB-I without pre-peak derived from $I_C(2\theta)$ of Figure 4a (à); (c) $F(K)$ of background; (d) $F(K)$ of EB-II, derived from $I(2\theta)$ of Figure 6.

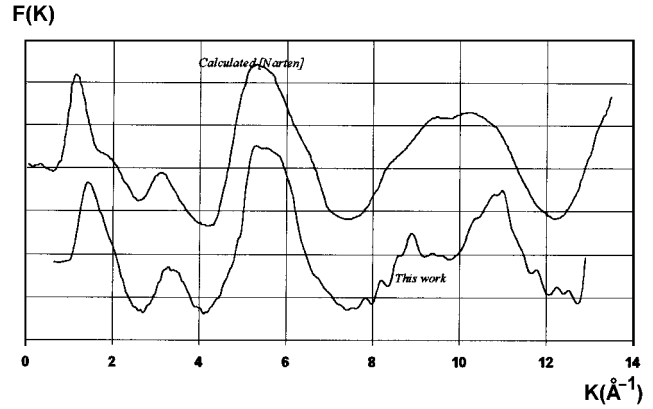

Fig. 8. In this figure two reduced interference functions are compared: (a) theoretical reduced interference function of liquid benzene proposed by Narten [20]; (b) the reduced interference function of polyaniline in the film form of EB-II washed with NMP solution.

doped then dedoped is approximately the same (3.4 Å^{-1}) (*cf.* [9,10]). But their height and profile behaviour is totally different. For example in the interference function of the *coherent background* (Fig. 7c) the profile indicates a shoulder on the small K side (2.8 Å^{-1}). This is contrary to its third peak which has the same height and the same maximum position (5.7 Å^{-1}). The height of this peak is greater than the first and the second peak, and its profile is very similar to liquid benzene (see Fig. 8) and amorphous carbon black (see $F(K)$ of amorphous carbon in Ref. [23]). On the other hand, it was previously reported [20] that the local order in liquid benzene is the same as crystalline solid benzene, as mentioned for the amorphous emeraldine base [9,10].

This structural analogy permits us to conclude that the pure amorphous EB, *i.e.* without the pre-peak or the line reflection on the X-ray pattern, is essentially a homogeneous single phase similar to that which was reported for liquid benzene.

However, the scattering from polyaniline (polymer) produces different X-ray diffraction patterns, diffuse halos, diffuse halos with pre-peak and lines superimposed on broad halos. This is contrary to the interference function of liquids which only have diffuse halos. These experimental facts do not advocate the two phase system model; especially in the presence of scarce Bragg reflections that have profiles which vary by increasing 2θ. Therefore it is vital to postulate a random array model where the structural elements are randomly arranged. The concept of crystallinity [14], which is evidence for the two phase concept, should be questioned for these materials.

In the present work, the contribution of the diffuse components was interpreted more carefully by a procedure of separating sharp lines from the diffuse halos. This diffuse coherent halo was then related to the X-ray pattern of a disordered "*reference state*" of polyaniline. The broadness of the principal peak in $F(K)$ (of the background) represents the randomness of this homogeneous isotropic state (Fig. 7c). The analysis of the interference functions of the background at the half maximum peak breadth, of the profile and each peak position indicates the existence of randomly arrayed chains. This homogeneous and isotropic state evolves to change the randomness (degree of disorder) of polyaniline. This evolution is produced by a *continuous transition* and such a *transition* is produced by choosing a convenient preparative method or by washing different samples (see Figs. 6 and 4a).

6 Analysis of the pre-peak

On the X-ray pattern, the scattering of structural evolution may appear in the form of a pre-peak before the principal peak (Fig. 7a). The pre-peak is one of the indications of medium range correlation. Its existence should be distinguished from the other manifestations of medium range order (MRO). The presence of the pre-peak is one of the more controversial aspects of the structural study of amorphous materials. This type of correlation generally arises from a variety of causes:

(a) cluster formation *e.g.* covalent AX2 glasses (*cf.* [24]);
(b) chemical ordering in a disordered material *i.e.* metallic glasses *e.g.* the amorphous Gd–Y system [26];
(c) the dihedral distribution effect [25].

The scattering of such a "structural evolution" on the X-ray pattern, as was mentioned above, may appear, before the principle diffuse peak in the form of a pre-peak. The pre-peak is usually sharper than the principle peak. Only simplistic models of polyaniline have been proposed due to incomplete structural information on polyaniline. Therefore, to study the pre-peak's origin and that of the medium range structural organisation in polymers an appropriate structural model is needed. If the Ehrenfest equation [27] ($d = 1.22(2\lambda)/K_{max}$) is used instead of the usual Bragg formula then K would be related to the maximum position of the pre-peak in K space where the "d" spacing is found to be 9 Å. Such a distance suggests that the reflection produced by the "inter-layer" interference, may be approximately six times the C–C distances. On the other hand, the correlation length, D, of this medium range organisation can be calculated by the Scherrer equation ($D = K\lambda/B\cos\theta$, where $K = constant = 0.9$, λ is the wavelength of the X-ray beam, B is the broadening of the pre-peak measured at half maximum peak breadth, and θ is the Bragg angle of the pre-peak). The correlation length (D), was found to be 28 Å which is twelve times that of the benzene ring in polyaniline or approximately five times the monomer unit.

In the Guinier patterns that show the presence of the pre-peak, a diffuse scattering near the direct beam is seen. This diffuse scattering disappears with the absence of the pre-peak (Fig. 5). The generation of a non homogeneous domain in the disordered intermeshed chain of polyaniline is indicated by the diffuse scattering at small angles. This domain may be generated in the middle of a random intermeshed chain of polymers in the form of two-dimensional layers which diffract the X-ray beam

in the form of the Bragg reflections or spectrum lines. The profile of these lines is not Gaussian; the profile of the two first lines are narrow and symmetrical, the third line is narrow with an enlarged foot and finally, at $2\theta > 25°$, lines are in the form of the diffraction bonds. This experimental fact, consisting of limited Bragg lines and shape of the lines, leads us to suggest that in the middle of a random intermeshed chain of polyaniline (polymers) there are locally two-dimensionally layered structures which scatter the X-ray beam in the form of the semi-Bragg reflections or line spectrum. Therefore suggesting that the reflection of the two-dimensional layered domain (*cf.* Fig. 4c) could be the origin of the polyaniline line spectrum. It must be mentioned that under circumstances with scarce reflection lines and with particular profiles, indexing these few lines would not allow the identification of the crystalline atomic arrangement (structure). Thus, the crystallite fraction cannot be estimated. In sum, the samples that are converted from EB-I powder to EB-II powder have a "structural evolution" that appears in the form of lines superimposed on broad halos. When NMP is used, for the samples in the film form, then a pre-peak is not even seen.

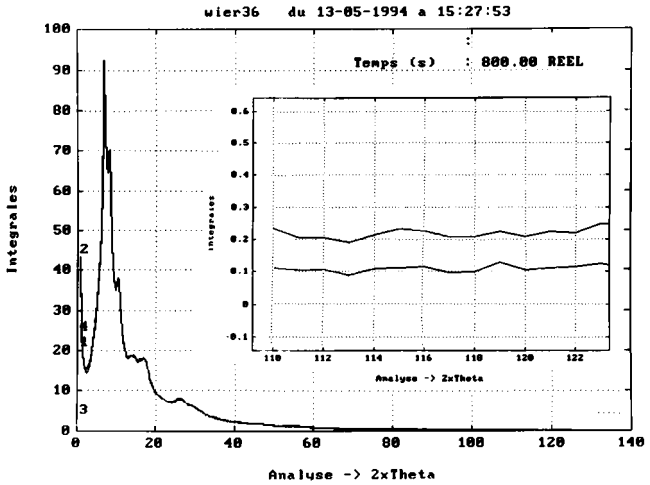

Fig. 9. This figure shows the reliability of intensity measurement using this novel technique (A.D.) in which the signal and behaviour of $I_C(K)$ even with high K values, is still the same in two different experiments (a and b). This comparison demonstrates how the data filling criteria are efficient in this novel experimental set-up.

7 The reduced radial distribution function

Another approach for describing the structure of polyaniline, in terms of crystalline atomic arrangements, is the determination of the reduced radial distribution function. In our previous work, this technique was known, as amorphography. For the first time, in the case of pure amorphous polyaniline, this technique has been used for determining SRO, MRO and the number of the nearest neighbouring atoms in atomic shells. The implementation of amorphography requires the experimental acquisition of appropriate diffraction data associated with analysis. In order to interpret quantitatively the RDF up to high order shells, many precautions and improvements have been undertaken in this work.

The structural information for disordered materials can be determined from real signals of medium range order (short range connectivity in terms of rings and dihedral angles) in K space. In principle, the recording of photons should be free of noise, *e.g.* statistical noise. However, for light materials this approach causes several problems. In order to avoid the statistical problems we scanned all the angular domains simultaneously, at the expense of counting statistics. We have repeated the number of scans in order to improve the statistics and reliability of the results.

To improve the reliability of X-ray patterns for each sample the reproducible data were added together. This rigorous data filtering criteria is certainly efficient as the X-ray pattern, $I(2\theta)$, of EB-II indicates in Figure 9.

Figure 10 shows the feature of four RDFs corresponding to the reduced interference functions of Figure 7. They vary slightly with different samples. These curves have the same common features: namely the position of the first four maxima. The maxima correspond to C_1–C_2 = 1.4 Å, C_1–C_3 = 2.4 Å, C_1–C_4 = 2.95 Å and C_1–C_5 = 4.3 Å distances respectively (*cf.* Fig. 10). The analysis of liquid benzene's RDF, $W(r)$, according to equation (5), demonstrates that the same (1.4, 2.44, 2.88, 4.3 Å) distances are obtained. In the case of liquid benzene these distances with other structural parameters, were sufficient to produce a good fit of the theoretical interference with the experimental function [20].

As mentioned in the preceding section, the reduced interference function of benzene is in agreement with the interference function of *pure amorphous polyaniline*.

In previous work [10], the analysis of RDFs has been performed by assuming that the $W(r)$ of amorphous polyaniline consists of two hypothetical partial RDFs: $W_1(r)$ and $W_2(r)$.

$W_1(r)$ is responsible for the interatomic distances of the atoms covalently bonded (distances are as mentioned above). The $W_2(r)$ for polyaniline and liquid benzene produces the interatomic distances of the intrachain or the topological distances. The peaks where (r) is greater than 3 Å corresponds to these distances.

In the case of the hypothetical partial RDF, where $W_1(r)$ is the one-dimensional network of the long chain composed of C–C or C–N, each carbon atom along the chain is bonded in a tetrahedral fourfold-coordination. Each carbon atom has two carbon neighbours along this polymer backbone (topological one-dimensional) and the third neighbour is an H atom which cannot be identified by X-ray diffraction methods. The fourth neighbour is H, N or C of the benzene ring *side group*.

Table 2 shows the agreement of interatomic distances up to 4 Å in the different polyanilines. The similarity of these values confirms the similarity of the skeleton of a single extended polyaniline with emeraldine washed, unwashed and dedoped in the form of powder or film.

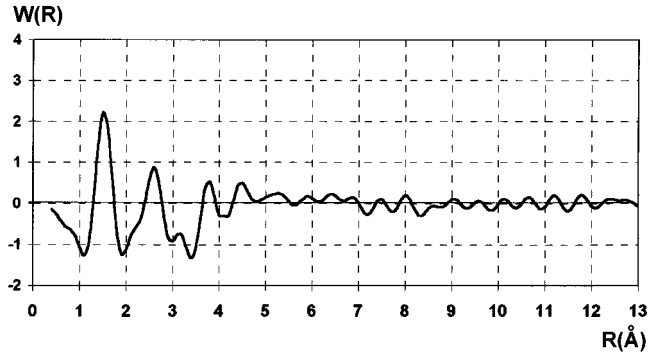

(a)

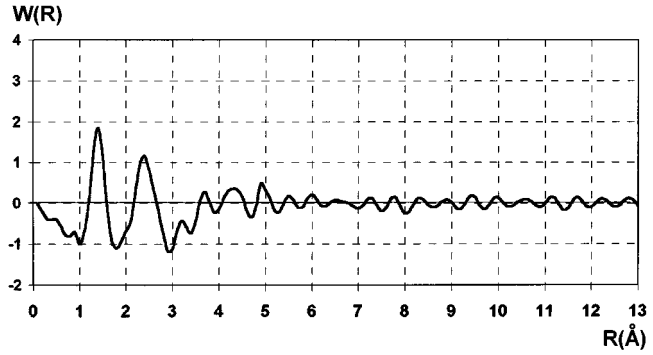

(b)

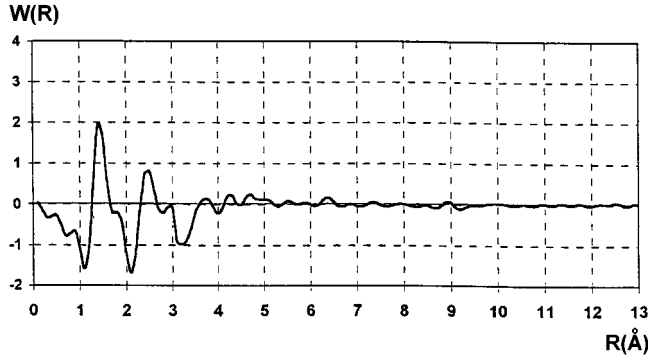

(c)

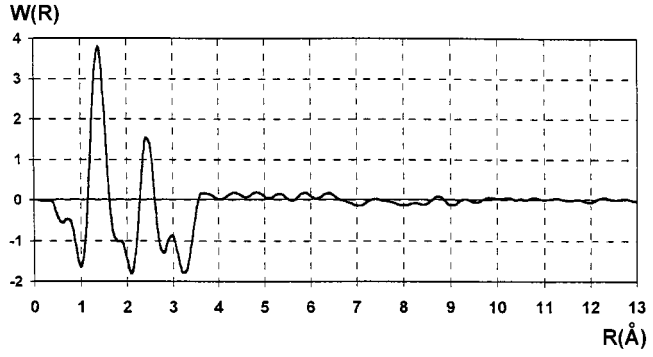

(d)

Fig. 10. The reduced radial distribution function derived by Fourier transform of the interference function of Figure 7.

Table 2. Interatomic distances derived from the reduced radial distribution of different samples. This table shows the similarity between interatomic distances of different samples up to 4 Å (see Fig. 10).

n	Powder (EBI)	Powder*** (EBI)	Film** (EBII) [5]	B.G. of powder* (EBII)
1	1.4	1.4	1.4	1.4
	1.9****	1.9****	-	-
2	2.4	2.4	2.4	2.4
3	2.86	3.1	2.95	2.95
4	3.7	-	-	-
5	4.25	4.25	4.32	4.3
6	-	-	4.83	-
7	5	5.5	5.4	-
8	-	6	5.8	-
9	-	-	6.4	-

* BG = background of X-ray diffraction of sample in form of powder, washed with THF.
** A new sample from EB-I washed with NMP solution.
*** Other preparation of EB-I.
**** Distances arising from the termination effect of integration – for integration limits of less than 15 Å this artefact disappears.

It is worth noticing that the radial distribution function derived from $F(K)$ of the coherent background gives the same three principle maxima and the other oscillations vanish more rapidly (Fig. 10c). This behaviour suggests that the total radial distribution function, $W(r)$, of the *reference state* is similar to the hypothetical partial radial distribution of the atomic backbone or the skeletal chain of polyaniline. In this curve the artefact distances of $r = 1.9$ Å which appear usually as a shoulder on the higher side of the first peak is eliminated by improving the acquisition technique and changing the upper limit of the integration $K_{max} = 20$ Å^{-1} to $K_{max} = 15$ Å^{-1} (*cf.* Eq. (5)). Thus it can be concluded that this sub-peak in the RDF of polyaniline has no physical meaning (*cf.* Fig. 10).

The carbon atoms 1, 2 and 3 on the backbone of the polymer define a plane. The position of carbon 4 is on a "zig-zag" plane which occurs due to the variation in the angles of rotation Φ. By changing Φ by a small range ($\delta\Phi$ as an operator) the skeleton of the carbon chain will continue to "zig-zag" all along the chain.

It is quite obvious from what has been discussed that the experimental results, at first approximation, correspond to the Random Coil Model proposed by Flory for glassy polymers. Flory uses this manner of chain construction to define his spatial configuration of random array model of macromolecular isolated chains [28]. This model of defining spatial configuration can also be applied in determining the spatial configuration of polyaniline's backbone. The essential part of this model consists of an ideal individual chain, energy free of other chains and unperturbed by the presence of neighboring chains *i.e.* the configurations are topologically one dimensional, such a

model is considered as a random coil configuration [30]. Therefore from these chains a configuration cognate to a 3-dimensional polymer structure can be imagined. If this is assumed, then $W(r)$ of the polyaniline background or the *reference state* can be considered as a partial pair-pair correlation function of the Random Coil model proposed by Flory.

In order to explain the structure of polymer glasses the one-dimensional configuration has been extended for the purpose of using the random coil model. The random coil model is essentially a homogeneous single phase model similar to that proposed for the continuous random network (in glass, vitreous silica) and the random close packing model of metallic glasses. The random coil model, like the two former models, has been the subject of numerous structural studies [29]. However, the main conflict in the structural studies of the two former models was the competition between the heterogeneous model of a *micro-crystalline* and homogeneous disordered network.

The generalised picture of these two examples corresponds best to a random array model where the structural elements are randomly arranged. Within such an array no structural unit with regular intervals has been reported. On the other hand, the following factors indicate the existence of a random array chain: the analysis of the interference function of the background, at the half-maximum peak breadth, the profile, the position of each peak and the RDF derived from the $F(K)$ of the background.

Thus, this novel X-ray diffractometry solves the conflict between microcrystalline and random array chain structures by analysing the coherent background. These results enabled us to choose a standard state of disorder in polyaniline (polymer). We consider that this homogeneous isotropic state of randomness can be taken as the *edge of disorder*. By defining this state of randomness, it can be seen that the atomic arrangements of long and fast changing structural chains are best fit to the random array model than the two-phase system model.

We are aware that the total RDF represents the one dimensional polymer structure and deducing the topology of the polymer from the total RDF would not be possible. Therefore it is vital to obtain the experimental partial distribution function. The new technique of anomalous diffractometry [31] allows us to obtain the partial interference function and partial radial distribution functions. The structure of polyaniline and the atomic configuration of any amorphous material can be defined by comparing the theoretical and the experimental RDF's and $F(K)$'s to each other (*cf.* [32]). Since the total RDF represents only the position dependence of the average atomic density, it cannot be used to establish a unique set of atomic coordinates from which the SRO's topology could be deduced.

In the case of some polymers the experimental partial radial distribution functions cannot be obtained since the K absorption edge of the light atoms in these compounds would not be experimentally accessible. For example the energy of the K edge of nitrogen is $E = 409$ eV which is not convenient for any X-ray diffractometry technique. On the other hand, it is known that a good resolution in the RDF functions needs a short wavelength in order to have a large K_{max} value. However, introducing an isomorphous substitution of a heavy ion the value of the K absorption edge can be increased (*e.g.* the K absorption edge of Cu is $E = 8\,979$ eV). This approach should be feasible as long as the heavy substituted ions do not alter the polymer's structure.

Therefore the best method to obtain the partial interference function is to have three different interference functions, $J(K, \omega)$, with three different scattering wave vectors with a very large K (as discussed in Sect. 2 and in detail Ref. [31,32]). Then Fourier inversion can be used to identify partial radial distribution functions.

In this work, each time the mode of preparing polyaniline was changed a *continuous variation* was observed in the degree of disorder in the atomic contribution of polyaniline . Therefore, polyaniline is a good prototype for the heavy-ion substitution procedure. The heavy atoms scatter differently with different energies, near and far from the absorption edge. In each case, the individual partial interference function can be obtained. The partial distribution function can be derived from these partial interference functions as mentioned in reference [31]. These functions vary with different degrees of disorder when the sample preparation has been changed to obtain different polyanilines. The information on the atomic distribution functions, in real space is given by the Fourier transformation of each partial $F(K)$. These pieces of information obtained for the nearest neighbouring atoms and the distances obtained between the heavy and the light atoms allow us to have a vision of the development of disorder and hence an appropriate picture of Flory's Random Coil Model.

On the other hand by using this technique (A.D.) the radius of gyration (*i.e.* $\sqrt{s^2}$) of these labelled domains can be obtained at different energies in different classes of polyanilines. This can be related to the displacement length of a chain (*i.e.* $\sqrt{r^2}$). By knowing this value we can develop a structure of a polymer at the edge of disorder.

8 Summary

By defining a reference state of randomness a new edification of notation for the structure of polyaniline (polymers) has been proposed. The interference function and the radial distribution function of this state of reference near the edge of disorder have been identified. It has been shown that in a random array chain network this state evolves in a "*continuum transition*" way to a non-crystalline state.

The X-ray patterns of each state have been obtained by the "Anomalous Diffractometry" (A.D.) method. The degree of disorder is obtained by comparing the profile of the first halo, existence of the pre-peak and the superposition of the lines on the background. The determination of the degree of disorder allows one to compare and relate samples that have been treated diversely or have different physical properties. For a network of compact long chains

of non-crystalline material such polyaniline (polymers) it is not possible to determine an X-ray diffraction pattern of the crystalline state. Therefore, this recent manner of classification is more useful and meaningful in contrast to the traditional way of measuring crystallinity. It is difficult to imagine an ideal crystalline state in the middle of a network of long compact chains of non-crystalline material such as polyaniline. Also the anomalous diffractometry (A.D.) method may be used to study autocatalysis in the network of long dense chain materials, such as polymers.

We are grateful to Dr. F. Dénoyer for her useful discussions and would like to thank Mr. J.P. Wagner for his technical assistance.We would also like to thank companies such as "the Development Analyses and Measures and Maison Internationale de l'information" for their generous technical assistance. The authors would like to thank Dr. M.E. Josefowicz for preparing some of the samples used in this study. Also we thank Mr. G.Y. Min in Dr. A.G. MacDiarmid Laboratory for providing new samples. Finally, the realisation of this X-ray complex would not have started without Dr. S. Megtert providing funds for it for which we are we are very grateful. We would like to express gratitude to Dr. C. Rosser and Miss N. Hooper for reading this manuscript in a critical manner.

References

1. A.J. Epstein, J.M. Ginder, F. Zuo, R.W. Bigelow, H.S. Woo, D.B. Tanner, A.F. Richter, W.S. Huang, A.G. MacDiarmid, Synth. Metals **18**, 303 (1987).
2. A.G. MacDiarmid, A.J. Epstein, Faraday Discussions, Chem. Soc. **88**, 317 (1989).
3. A.G. MacDiarmid, A.J. Epstein, Synth. Metals **65**, 103 (1994).
4. F. Zuo, M. Angelopoulos, A.G. MacDiarmid, A.J. Epstein, Phys. Rev. B **39**, 3570 (1989).
5. A.J. Epstein, J.M. Ginder, F. Zuo, R.W. Bigelow, H.S. Woo, D.B. Tanner, A.F. Richter, W.S. Huang, A.G. MacDiarmid, Synth. Metals **18**, 303 (1987).
6. J. Joo, A.J. Epstein, V.N. Prigodin, G.Y. Min, A.G. MacDiarmid, Phys. Rev. B **50**, 12226 (1994).
7. M.E. Jozefowicz, R. Laversanne, H.H.S. Javadi, A.J. Epstein, J.P. Pouget, X. Tang, A.G. MacDiarmid, Phys. Rev. B **39**, 12958 (1989).
8. J.P. Pouget, M.E. Jozefowicz, A.J. Epstein, X. Tang, A.G. MacDiarmid, Macromol. **24**, 779 (1991).
9. M. Laridjani, J.P. Pouget, E.M. Scherr, A.G. MacDiarmid, M.E. Jozefowicz, A.J. Epstein, Macromol. **25**, 4106 (1992).
10. M. Laridjani, J.P. Pouget, A.G. MacDiarmid, A.J. Epstein, J. Phys. France **2**, 1003 (1992).
11. M. Laridjani, P. Leboucher, D. Raoux, J.F. Sadoc, J. Phys. France **46**, 157 (1985).
12. A. Guinier, G. Fournet, *Small-angle scattering of X-ray* (Wiley, New York, 1955).
13. A. Guinier, *Théorie et Technique de la Radiocristallographie*, 3rd edn. (Dunod, Paris, 1964).
14. L.E. Alexander, *X-ray Diffraction Method in Polymer Science* (Publishing John Wiley, 1964), chap. 3.
15. W. Ruland, J. Appl. Phys. **4**, 70 (1971); Acta Cryst. **14**, 1180 (1961).
16. B.K. Vainshtein, *Diffraction of X-ray by chain molecules* (Publishing Elsevier, 1966), p. 370.
17. C.G. Vonk, J. Appl. Cryst. **6**, 148 (1973).
18. M. Laridjani, J. Phys. I. France **6**, 1347 (1996).
19. W. Gander, J. Hrehicer, *Solving problem in scientific computing using maple and MATLAB* (Publishing Springer, 1992).
20. A.H. Narten, J. Chem. Phys. **18**, 1630 (1969).
21. E.G. Cox, D.W. Crulckshank, A.S. Smith, Proc. Roy. Soc. Lond. A **247**, 1 (1958).
22. J.D. Bernal, Proc. R. Soc. **37**, 355 (1959).
23. H.P. Klug, L.E. Alexander, *X-ray diffraction, Procedures for polycrystalline and amorphous material* (Publishing John Wiley, 1973).
24. S.R. Elliot, Phys. Rev. Lett. **67**, 711 (1971).
25. S.R. Elliot, J. Non-Cryst. Solids **97**, 159 (1987).
26. M. Laridjani, J.F. Sadoc, J. Phys. France **42**, 1293 (1981).
27. A. Guinier, D.L. Dexter, *X-ray studies of Material* (Publishing John Wiley, 1963).
28. P.J. Flory, *Principles of Polymer Chemistry* (Cornell University Press, Ithaca, 1953), Chap. X.
29. D.R. Uhlmann, J. Non-Cryst. Solids **42**, 119 (1980).
30. P.J. Flory, Science **188**, 1268 (1975).
31. M. Laridjani, J.F. Sadoc, D. Raoux, J. Non-Cryst. Solids **91**, 217 (1987).
32. M. Laridjani, , J.F. Sadoc, J. Phys. France **50**, 1953 (1989).